THE ASTRONOMICAL JOURNAL VOLUME 109, NUMBER 2 FEBRUARY 1995

INFRARED SPECTRAL ENERGY DISTRIBUTIONS OF YOUNG STELLAR OBJECTS IN BOK GLOBULES

JOÃO LIN YUN
Departamento de Física, Universidade de Lisboa, Campo Grande, Edif. C1, 1700 Lisboa, Portugal
Electronic mail: yun@delphi.cc.fc.ul.pt

DAN P. CLEMENS
Astronomy Department, Boston University, 725 Commonwealth Avenue, Boston, Massachusetts 02215
Electronic mail: clemens@protostar.bu.edu

Received 1994 July 13; revised 1994 October 17

ABSTRACT

We present near-infrared photometry from a J, H, and K-band imaging survey towards *IRAS* sources in Bok globules. Analysis of the photometry provided near-infrared magnitudes, fluxes, and colors of these YSOs. Using the near-infrared colors together with the coordinates of the objects, the most likely near-infrared counterparts to the *IRAS* far-infrared point sources are identified. Broadband spectral energy distributions (SEDs) for the YSOs were established and the sources were classified according to the shapes of their SEDs. Of the 22 *bona fide* YSOs found, 10 are Class I. Half of the remaining 12 sources are classified as Class II and the other half as Class II-D. We find that the Class I sources seem to be particularly well identified by the 12/25 μm spectral index. For Class I and Class II sources, the 12/25 μm spectral index and the 2/25 μm spectral index both give the same information about the embeddedness and type of YSO.

1. INTRODUCTION

Bok globules are the simplest and least massive molecular clouds in the galaxy. As such, they are constrained to be the sites of only low mass star formation. They offer a uniquely clean laboratory in which to study star formation away from confusing processes such as shocks, winds, and triggered star formation.

Until recently, only a handful of globules were known to lodge young stars. In our *IRAS* survey (Yun & Clemens 1990) we found that a surprisingly large number of Bok globules show evidence for associated far-infrared point sources. Follow-up studies proved these to be *bona fide* young stellar objects (Yun & Clemens 1992, 1994b).

In one of those previous studies (Yun and Clemens 1994b), the data acquisition and analysis of a near-infrared survey of YSOs in Bok globules were presented. Furthermore, the results of a visual examination of the resulting images were described, including an analysis of the morphology of the near-infrared nebulosities found to be associated with 11 YSOs.

In this paper, the natures of the YSOs in Bok globules are further explored via detailed investigation of the near-infrared magnitudes and fluxes using synthetic aperture photometry applied to the near-infrared array images discussed in Yun & Clemens (1994b). Combining these data with *IRAS* fluxes, spectra energy distributions of these objects between the wavelengths of 1 and 135 μm were constructed and analyzed.

Lada and collaborators (e.g., Lada & Wilking 1984; Adams *et al.* 1987; Lada 1988) have found that broadband infrared spectral energy distributions (SEDs) are able to reveal much about the physical nature of low-mass YSOs. Lada & Wilking (1984) divided low-mass YSOs into three morphological classes based on the shapes of the observed SEDs and on the values of the corresponding spectral indices α. We adopt here the definition of Adams *et al.* (1987) for the spectral index of a YSO, i.e., $\alpha = d \log(\nu S_\nu)/d \log \nu$, where ν is the frequency and S_ν the flux density.

Class I sources exhibit SEDs that are broader than a single blackbody function. The SEDs of these sources rise with increasing wavelength from near-infrared to far-infrared and their spectral indices α are negative. This type of energy distribution resembles those predicted for accretion objects, i.e., protostars surrounded by an infalling envelope (Adams & Shu 1986; Adams *et al.* 1987). Typically, such sources do not have optically visible counterparts (e. g., Lada & Wilking 1984; Myers *et al.* 1987).

Class II sources have SEDs that are also broader than a single blackbody function, but have positive values of α, typically in the range of 0 to 1, with mostly flat-topped SEDs. These sources are usually associated with optically visible T Tauri stars (e.g., Lada 1991; Rucinski 1985). The infrared emission in excess of the stellar photospheric radiation is thought to be produced in a circumstellar disk (Rucinski 1985; Rydgren & Zak 1987) with a temperature distribution which is a power law with distance from the star. There is also evidence that Class I sources (obscured sources) evolve to become Class II sources (visible T Tauri stars) (e.g., Myers *et al.* 1987).

Class III sources have large positive values of $\alpha \sim 3$, with SED widths comparable to those of a single blackbody function and consistent with the SEDs expected from reddened stellar photospheres.

A subgroup of Class II sources have also been identified: Class II-D sources have a double-peaked energy distribution. Typically the peaks occur at wavelengths of around 1 and 60

 0004-6256/95/109(2)/742/10/$0.90

μm, indicating the presence of both warm ($T\sim3000$ K) and cool ($T\sim50$ K) dust.

The major goals of this near-infrared imaging survey of star forming Bok globules were two-fold. The first goal was to identify the most likely near-infrared stellar counterparts to the far-infrared *IRAS* point sources in these clouds. The second goal was to develop and classify the SEDs of these young stars.

In Sec. 2, we describe the photometry performed. The process of identification of the near-infrared counterparts of the YSOs is described in Sec. 3. A catalog of counterparts is presented in that section also. In Sec. 4 the resulting SEDs are presented and the sources classified. In the remaining sections the results are discussed and summarized.

2. PHOTOMETRY

The details of the initial data reduction (flatfielding and mosaicking) were described in Yun & Clemens (1994b). The final mosaics covered a total area of about 7.5×7.5 arcmin^2 (for the NICMOS 3 array) or 6×6 arcmin^2 (for the SQIID array). In both cases, we restricted our attention to a central area of about 4.′5×4.′5 which had reduced background noise level σ (typically about 21 mag per sq arcsec) compared to the remaining area.

To obtain the photometry of the stars contained in the central regions of the final, reduced images, standard IRAF[1] routines were used. First, the routine DAOFIND was used to identify stars with a minimum signal-to-noise ratio of 5. Next, the fluxes of these stars through a set of apertures (of 2.7, 4.5, 6.3, 9.0, and 10.8 arcsec radii) were measured using the IRAF aperture photometry routine APPHOT.

To avoid contamination from nearby stars, the fluxes obtained in the smallest aperture were used and corrected for the fact that they might not include all the flux from a star. The correction was based on computing, for the brightest stars in each frame, the mean and the dispersion of the differences between the magnitude obtained in the first aperture and the magnitudes obtained in each of the other apertures. Given that the third aperture (6.3 arcsec radius) was found to include virtually all (99%) of the flux from these bright stars, the magnitude of a typical star was taken to be the magnitude obtained in the first aperture corrected by the mean of the difference between the magnitude in the first and in the third apertures for the bright stars. Finally, experiments with different aperture sizes were performed. We concluded that changing the aperture sizes did not dramatically alter the photometric results and uncertainties.

Observation of standard stars (Elias *et al.* 1982) allowed correcting the resulting instrumental magnitudes for atmospheric extinction (to airmass=0) and subsequently to perform transformations to the Johnson standard system (Johnson *et al.* 1968).

Six standard stars were observed in 1991 May with the NICMOS 3 near-infrared camera (Rieke *et al.* 1989; Thompson *et al.* 1989). In 1991 November, seven standard stars were observed with the SQIID near-infrared camera (Ellis *et al.* 1992).

[1]IRAF is distributed by National Optical Astronomy Observatories which are operated by the Association of Universities for Research in Astronomy, Inc., under contract to the National Science Foundation.

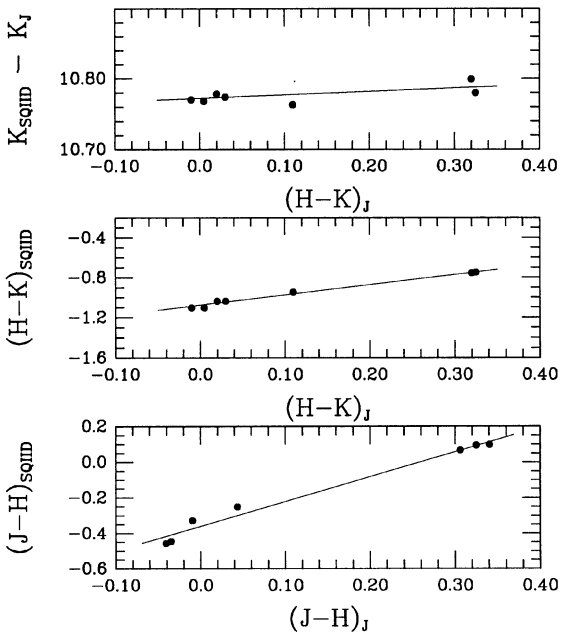

FIG. 1. Transformation from the SQIID instrumental magnitudes and colors to the Johnson standard system, according to Eqs. (4) to (6).

The IRAF APPHOT aperture photometry routine was used with the zero point of the instrumental magnitude scale (magnitude of a star with 1 count in 1 second of integration time) set to 26. The transformations between instrumental magnitudes and magnitudes in the Johnson system were found to be:

$$K_{\rm NICMOS}=K_J+7.251-0.180(H-K)_J, \quad (1)$$

$$(H-K)_{\rm NICMOS}=-0.431+0.919(H-K)_J, \quad (2)$$

$$(J-H)_{\rm NICMOS}=0.458+1.003(J-H)_J, \quad (3)$$

and

$$K_{\rm SQIID}=K_J+10.743+5.04\times10^{-2}(H-K)_J, \quad (4)$$

$$(H-K)_{\rm SQIID}=-1.086+0.927(H-K)_J, \quad (5)$$

$$(J-H)_{\rm SQIID}=-0.355+0.809(J-H)_J. \quad (6)$$

As an example of the transformations, Fig. 1 shows the fit of the SQIID data to the Johnson standard system. The corresponding NICMOS plots look similar. Figure 2 shows the residuals to the fits. The residuals are $\leq$0.05 mag (mostly$\leq$0.02).

These transformations were used to de-extinct and transform the instrumental magnitudes of the stars contained in the images of the globules to the Johnson standard system.

A plot of the nominal, internal uncertainties σ, as a function of the Johnson magnitudes J, H, and K, for a typical SQIID image, is shown in Fig. 3. Uncertainties range from less than 5% for bright stars to ~20% for faint stars.

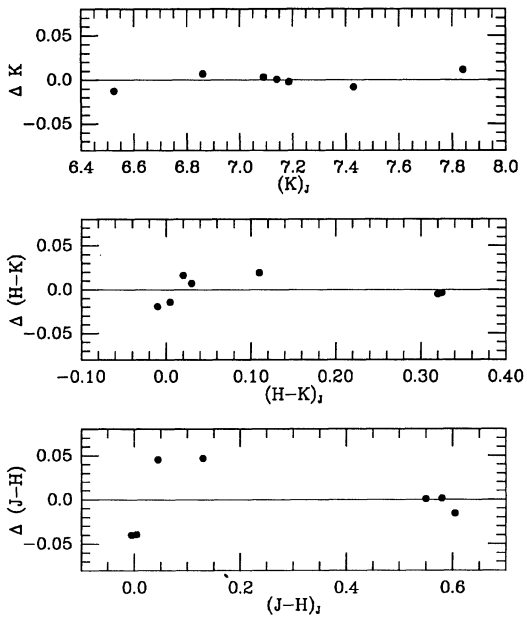

FIG. 2. Residuals of the transformation defined in Eqs. (4) to (6). Residuals are ≤0.02 except in $(J-H)$ where they are ≤0.05.

Figure 4 shows histograms of the magnitudes of the stars obtained for a typical image. We estimate the magnitude completeness of our images to be 16 at J, and 15 at H and K.

The magnitudes obtained were de-extincted and transformed to the Johnson standard system. Hereafter, all the magnitudes will be expressed in the Johnson system.

3. COUNTERPART IDENTIFICATION

In order to construct accurate SEDs of the YSOs, identification of the near-infrared counterparts of the far-infrared *IRAS* point sources is required. A procedure was adopted which identifies as near-infrared counterparts those stellar objects which show the presence of near-infrared nebulosity, have excellent spatial coincidence with the *IRAS* PSC

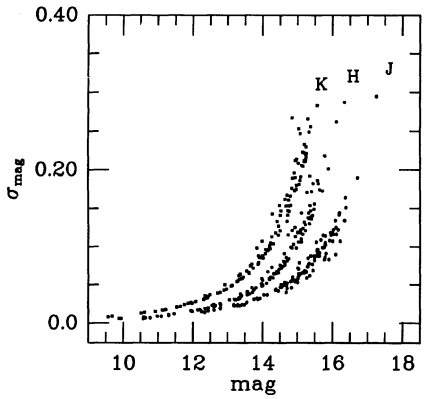

FIG. 3. Uncertainty σ as a function of magnitudes, J, H, and K. Uncertainties range from less than 5% for bright stars to ~20% for faint stars.

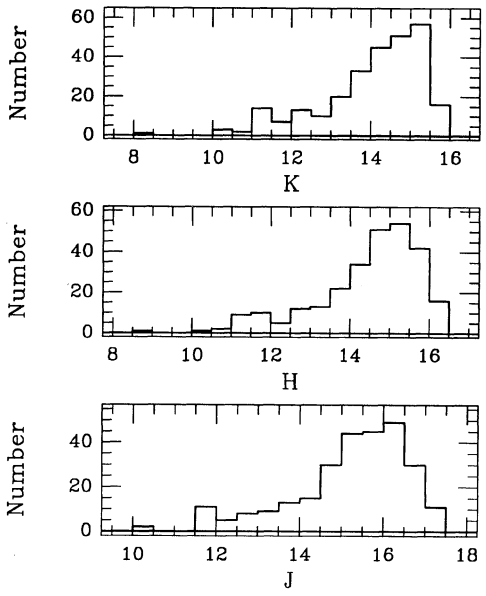

FIG. 4. Histograms of the magnitudes of the stars for a typical image.

sources, and/or show extremely red colors. However, it should be noted that the very coldest protostars (e.g., B335) may not exhibit detectable near-infrared emission (brighter than about 15 mag at K) and will be missed by this survey.

3.1 Methodology

The procedure used to identify the near-infrared counterparts consisted of three steps:

(1) Objects with associated near-infrared nebulosity were accepted as the near-infrared counterparts of the *IRAS* sources. Near-infrared colors and coordinates were also checked, as in steps 2 and 3 below. In the cases where no object was found to have associated nebulosity or where more than one object was found to have associated nebulosity, the following two steps were used to select the most likely counterpart.

(2) While inspecting the color–color diagram [the plot of the $(J-H)$ color versus the $(H-K)$ color; see below], the reddest objects [largest $(H-K)$] were identified. If these exhibited color indices indicative of the presence of circumstellar dust, their spatial positions were noted. These positions were examined to see whether they coincided with objects exhibiting nebulosity, and whether the positions were close to the *IRAS* PSC coordinates for the YSOs. Some objects were rejected if they were close to the edge of an image (outside a central area of 3×3 arcmin^2) or very faint (m_J>18), yielding very uncertain photometry.

(3) Because we expect cases where the objects need not be very red (e.g., objects with positive 12/25 μm spectral indices), and because sometimes the two previous steps failed to identify possible counterparts, a third procedure was applied. The colors of the stars in the vicinity of the *IRAS* PSC coordinates (starting with the closest and proceeding to more distant stars) were examined. If the color indices were indicative of the presence of circumstellar dust, their spatial

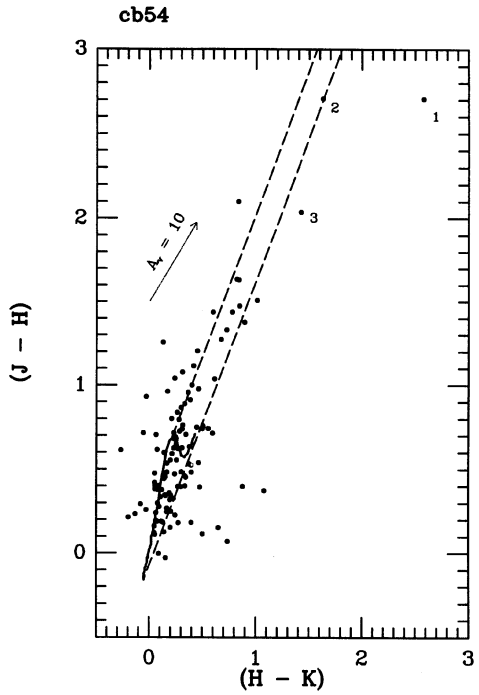

FIG. 5. Color–color diagram [$(J-H)$ vs $(H-K)$] obtained from the near-infrared images towards CB54YC1. The solid line (covered with filled dots) is the loci of unreddened main sequence stars (see Fig. 6). The two parallel, dashed lines define a reddening band where main-sequence stars will be located if extinguished by dust with standard properties. The dotted line shows the direction and length of the reddening vector for $A_V \sim 10$ mag. Objects 1, 2, and 3 are the best candidates to be the near-infrared counterpart of CB54YC1 (IRAS 07020−1618).

positions were noted. The objects were accepted as the near-infrared counterparts of the YSOs if the positions were within 1′ of the *IRAS* PSC coordinates. This value is close to the 3σ upper limit of the distribution of *IRAS* PSC error ellipse major axes, and represents a reasonably firm maximum likely separation.

As an example of this procedure applied to a simple case, the color–color diagram obtained from the near-infrared images towards CB54YC1 is presented in Fig. 5. In this figure, the $(J-H)$ colors are plotted vs the $(H-K)$ colors. The solid line is the location of the unreddened main sequence stars (Koornneef 1983). The two parallel, dashed lines define a reddening band where the main-sequence stars will be located if extinguished by dust with standard properties. The dashed lines assume the standard interstellar extinction law (e.g., Koornneef 1983). The dotted line shows the reddening vector corresponding to 10 mag of visual extinction. Unextincted giant stars occupy a region of the color–color diagram just above the solid line but still contained in the reddening band. Stars falling to the right of the reddening band have intrinsic infrared excess emission due to heated circumstellar dust and are thus more likely to be embedded objects (Lada & Adams 1992).

According to the procedure described above, the stars labelled 1, 2, and 3 were initially noted as possible counterparts because their color indices correspond to those of objects with large values of $(H-K)$. Checking the spatial coordinates of these objects and looking at the corresponding near-infrared images, objects 1 and 2 were found to be surrounded by common nebular emission (Yun & Clemens 1994b) and they are very red as indicated by their colors. One (or both) of these objects may be the near-infrared counterparts(s) of CB54YC1.

To determine the coordinates of these objects, stars appearing both in the near-infrared images and in the Space Telescope Guide Star Catalog were identified. After a coordinate transformation, object 2 was found to be located within 7″ of the *IRAS* PSC position (well within the uncertainties of the *IRAS* positions and of the coordinate transformation). Thus, object 2 is identified as the near-infrared counterpart of CB54YC1.

In a few globules, the reddest objects in the color–color diagram corresponded to stars located near the edges of the image (more than 3 arcmin away from the PSC coordinates) and were typically very faint. In these cases, the objects were rejected and the search continued to the next reddest object, checking its spatial position, as described in step 2 above. If this step also failed to identify possible counterparts, the search continued to the object closest to the *IRAS* PSC position, checking its colors, as described in step 3.

Using the procedure described above, near-infrared counterparts were found for 22 YSOs. This represents an overall success rate of 65% (22 identifications in a sample of 34 YSOs).

The group of 12 Bok globule YSOs whose near-infrared counterparts were not found is composed of: CB28YC1, CB35YC1, CB55YC1, CB81YC1, CB87YC1, CB90YC1, CB171YC1, CB180YC1, CB203YC1, CB206YC1, CB217YC1, CB248YC1. These objects are characterized by the following. Five YSOs are not present in the *IRAS* PSC catalog; they were detected only in the coadded images (Yun & Clemens 1990) and may be either significantly fainter at all wavelengths or represent less reliable YSO identifications than those contained in the PSC. Most (eight) YSOs have positive spectral indices $\alpha_{12/25} > 0.5$, and only two YSOs have $\alpha_{12/25} < 0$ (CB81YC1, CB87YC1). These "bluer" sources may have much smaller quantities of circumstellar dust and anisotropic scattering at near-infrared wavelengths, rendering them much fainter than their more deeply embedded, highly scattering cousins. Three YSOs are located in very crowded regions of the corresponding near-infrared images, where source confusion and/or contamination is very likely to occur. Here the lack of an unambiguous candidate makes SED construction difficult. There are too many potential counterparts and no way to identify those truly associated with the PSC source(s). The *JHK* images of two YSOs are of poor quality due to scattered light from the nearby moon (CB203YC1, CB206YC1). One or more of these aspects may have hampered the correct identification of the near-infrared counterparts of these 12 YSOs.

A general summary of the no-counterpart group is that source faintness and confusion have likely hampered the association process. We expect that with somewhat deeper near-infrared images and/or deep mid-infrared images, the fraction of associations would increase to near unity.

TABLE 1. Near-infrared survey of YSOs in Bok globules: near-infrared counterparts and photometry.

YSO/ Counterpart	R. A. (1950)	Decl. (1950)	Δ R. A. (″)	Δ Dec. (″)	Near-infrared photometry[a] K	$(J-K)$	$(H-K)$	Basis of ID	Notes
(1)	(2)	(3)	(4)	(5)	(6)	(7)	(8)	(9)	(10)
CB3YC1-I	$0^h26^m00.5^s$	56°25′36″	22	4	8.24	2.12	0.70	N,R,C	
CB6YC1-I	$0^h46^m34.2^s$	50°28′26″	−2	1	12.00	2.70	1.00	N,R,C	b
CB30YC1-I	$5^h26^m52.6^s$	5°38′05″	10	−10	12.54	2.12	0.88	R	c
CB31YC1-I	$5^h30^m45.6^s$	−0°38′16″	6	1	8.79	1.82	0.70	N,R,C	
CB32YC1-I	$5^h33^m47.8^s$	−0°19′04″	4	−1	7.14	1.42	0.85	N,R,C	
CB34YC1-I	$5^h44^m02.2^s$	20°58′59″	−10	−8	9.81	3.36	1.68	N,R,C	
CB39YC1-I	$5^h59^m06.4^s$	16°31′00″	7	2	6.71	1.94	1.13	RC	
CB50YC1-I	$6^h31^m34.5^s$	7°47′54″	−27	−16	11.73	1.11	0.38	R	
CB52YC1-I	$6^h46^m24.9^s$	−16°50′40″	−6	3	10.81	0.72	0.27	N,R,C	c
-II	$6^h46^m24.8^s$	−16°50′34″	−7	−4	12.62	2.18	0.86	N,R,C	c
CB54YC1-I	$7^h02^m06.2^s$	−16°18′40″	3	−7	11.76	4.34	1.63	N,R,C	
-II	$7^h02^m06.8^s$	−16°18′46″	12	−1	10.61	5.29	2.58	N,R,C	
CB60YC1-I	$8^h02^m37.7^s$	−31°22′00″	−7	−9	10.89	0.71	0.27	N,R	
-II	$8^h02^m38.4^s$	−31°22′03″	3	−6	13.39	1.77	0.69	N,R	
CB128YC1-I	$18^h13^m15.2^s$	−3°50′25″	15	−19	6.40	0.60	−0.40	R	d
CB142YC1-I	$18^h27^m11.5^s$	−13°43′03″	−9	−10	8.67	0.81	−0.37	R	d
CB188YC1-I	$19^h17^m54.1^s$	11°30′14″	2	18	10.88	3.01	1.28	NR	d
CB205YC1-I	$19^h43^m21.8^s$	27°43′40″	1	3	10.70	3.90	2.20	N,R,C	b
CB214YC1-I	$20^h1^m54.3^s$	26°30′29″	23	41	13.08	4.75	2.19	R	d
CB216YC1-I	$20^h03^m46.1^s$	23°18′37″	25	42	9.99	3.80	1.51	N,R	d
CB230YC1-I	$21^h16^m53.6^s$	68°04′54″	−12	2	10.81	3.51	1.33	N,R,C	
-II	$21^h16^m55.5^s$	68°04′53″	18	1	12.70	> 4	1.50	N,R,C	
CB232YC1-I	$21^h35^m14.5^s$	43°07′07″	1	2	11.93	5.55	2.67	R,C	
CB240YC1-I	$22^h31^m45.8^s$	58°16′24″	−2	−2	12.72	1.62	0.69	R,C	
CB244YC1-I	$23^h23^m50.5^s$	74°01′16″	25	9	13.90	3.30	1.10	R	
CB247YC1-I	$23^h55^m03.1^s$	64°30′07″	−8	−3	9.61	1.91	0.82	R,C	

Notes to TABLE 1

[a]Johnson system magnitudes and colors. The uncertainties are estimated to be between 0.05 mag (for brighter stars in uncrowded regions) to 0.25 mag (for fainter stars in crowded regions).
[b]The photometry includes contribution from the nebula.
[c]Coordinates derived from the telescope positioning. The uncertainties are estimated to be about 10 arcsec.
[d]Coordinates derived from the telescope positioning. The uncertainties are estimated to be about 30 arcsec.

3.2 Catalog of Counterparts

Table 1 presents the near-infrared counterparts found for the YSOs according to the method described. Column (1) identifies the infrared source. Columns (2) and (3) list the coordinates obtained from the near-infrared survey. CB52YC1, CB54YC1, CB60YC1, and CB230YC1 have two entries, one for each member of the binary (Yun & Clemens 1994b). Except where noted in the table (column 10), the positions listed for the near-infrared counterparts are tied to the *HST* GSC and have uncertainties estimated to be less than 2 arcsec. The exceptions consist of the frames in which it was not possible to identify stars appearing in the GSC. For these frames, the positions are based on telescope pointing, with uncertainties estimated to be between 10 and 30 arcsec, as noted.

Columns (4) and (5) list the offsets of the near-infrared sources from the *IRAS* positions.

Columns (6), (7), and (8) present the results of the near-infrared photometry. The 1σ relative uncertainties in the photometry are estimated to be between less than 5% for bright stars ($m_K<13$) in uncrowded regions of the images to about 25% for faint stars ($m_K>15$) in crowded regions of the images. Some sources of uncertainties are the quality of the near-infrared array images (flatfielding, defects, etc.), the noise level of the images, the goodness of the fit to the standard system, and the crowding in some areas of the images. In the remainder of this paper, our conclusions are not affected by these uncertainties.

Column (9) indicates the basis used for the identification of the counterpart. An "N" indicates that the counterpart is associated with infrared nebulosity. An "R" indicates a red object, according to the near-infrared colors in the color–color diagram. A "C" appears if the counterpart is within 10″ of the position listed in the *IRAS* PSC coordinates for the YSO candidate.

In general, given the uncertainties in the coordinates derived here for the near-infrared counterparts of the YSOs and the uncertainties in the *IRAS* PSC coordinates, we find good positional agreement between the *IRAS* PSC sources and our near-infrared counterparts. This positional coincidence, together with the previous evidence of YSO character (Yun & Clemens 1994b), is sufficient to identify these objects as *bona fide* YSOs.

4. BROADBAND SPECTRAL ENERGY DISTRIBUTIONS

In order to construct the broadband spectral energy distributions of the YSOs, from 1 to 135 μm, the photometry listed in Table 1 was combined with the fluxes presented in the *IRAS* PSC. These *IRAS* fluxes are listed in Table 2 to-

TABLE 2. Near-infrared survey of YSOs in Bok globules: *IRAS* PSC fluxes.

YSO	*IRAS* PSC fluxes (Jy)			
	12 μm	25 μm	60 μm	100 μm
CB3YC1	0.76E	1.12C	30.56A	~ 108.50A
CB6YC1	< 0.25M	1.01A	3.96A	8.96A
CB30YC1	< 0.25	< 0.25L	1.54B	12.08E
CB31YC1	< 0.25L	0.58B	< 2.64E	< 30.66D
CB32YC1	1.09B	1.47A	< 1.55J	~ 35.15B
CB34YC1	0.88	2.78	10.68	28.66
CB39YC1	4.53A	9.86A	7.27A	10.64A
CB50YC1	< 0.26I	< 0.35E	3.04C	~ 18.10C
CB52YC1	0.61A	0.80A	9.53A	38.41A
CB54YC1	0.57B	3.66A	43.34A	111.50A
CB60YC1	1.64C	2.39B	19.73B	~ 67.04A
CB128YC1	2.39A	1.31A	< 0.40E	< 16.66E
CB142YC1	0.95C	0.68B	< 10.18H	< 222.50B
CB188YC1	< 0.27K	1.06A	3.93B	~ 18.48B
CB205YC1	1.07A	4.91A	30.13A	~ 83.97B
CB214YC1	0.21E	0.52A	0.88B	< 21.58
CB216YC1	1.87A	5.57A	10.95A	17.65B
CB230YC1	< 0.25K	0.68A	11.75A	33.53A
CB232YC1	1.02A	3.55A	6.86A	~ 13.89A
CB240YC1	0.58A	0.76A	6.89A	22.47A
CB244YC1	< 0.25	0.78A	9.60A	15.20A
CB247YC1	0.32C	1.11A	1.63B	< 14.03

Notes to TABLE 2

The letters following each flux are the PS template codes, as follows: "A" =100% match with PS template, "B"=99% match, etc.

gether with the PSC correlation coefficients with the point source templates. Conversion from magnitudes in Table 1 to fluxes were based on the zero points of the Johnson system according to Koornneef (1983).

The resulting spectral energy distributions of the YSOs are displayed in Figs. 6(a), 6(b), 7, and 8. For the YSOs that may be binaries (two entries in Table 1), the SEDs plotted refer to the first Table 1 entry. Inclusion of the second object did not change the results of the source classification. In the plots of Figs. 6(a), 6(b), 7, and 8, filled circles correspond to flux values, open circles represent a lower quality detection (in the *IRAS* PSC catalog), and open circles with arrows represent upper limits. The sizes of the flux uncertainties in the plots are about one quarter of the sizes of the circles used to show the fluxes.

4.1 Source Classification

The YSO SEDs shown in Figs. 6(a) and 6(b) correspond to those of CB6YC1, CB34YC1, CB54YC1, CB188YC1, CB205YC1, CB214YC1, CB216YC1, CB230YC1, CB232YC1, and CB244YC1. These are all likely to be Class I sources. They exhibit SEDs rising rapidly towards longer wavelengths.

Figure 7 shows the SEDs of CB3YC1, CB30YC1, CB50YC1, CB52YC1, CB60YC1, and CB240YC1, which are likely to be Class II-D sources. Their SEDs exhibit two humps, one in the near-infrared and the other longwards of about 60 μm. However, observations at wavelengths of 5 and 10 μm (perhaps using ISO) are needed to confirm the Class II-D nature of these near-infrared counterparts to the *IRAS* sources.

Some cases (e.g., CB30YC1, CB240YC1) might also be classified as Class I sources. The existence of Class II-D sources that exhibit SEDs mixing features of Class I and Class II sources may confirm the idea that Class II-D sources

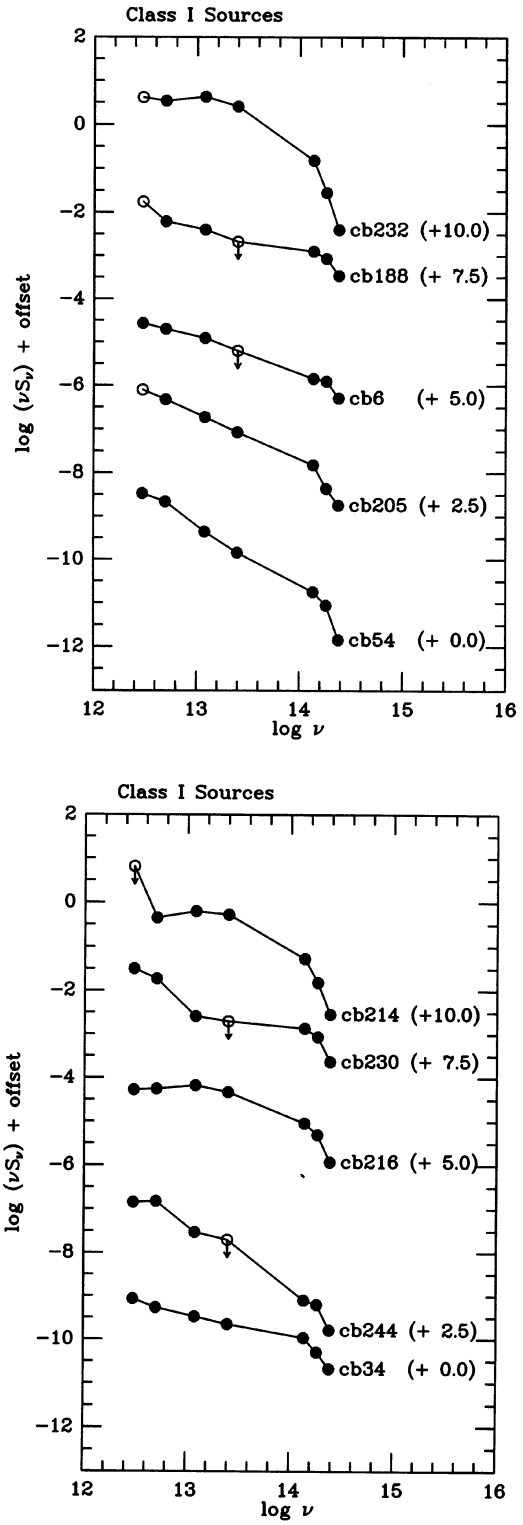

FIG. 6. Spectral energy distribution of the Class I YSOs. The number in parenthesis at the right, is the logarithm of the vertical offset of each SED.

are in transition between Class I and Class II, or that there is a continuous variation in the shapes of SEDs from Class I to Class III (Wilking *et al.* 1989), possibly due to projection effects (see Kenyon *et al.* 1993).

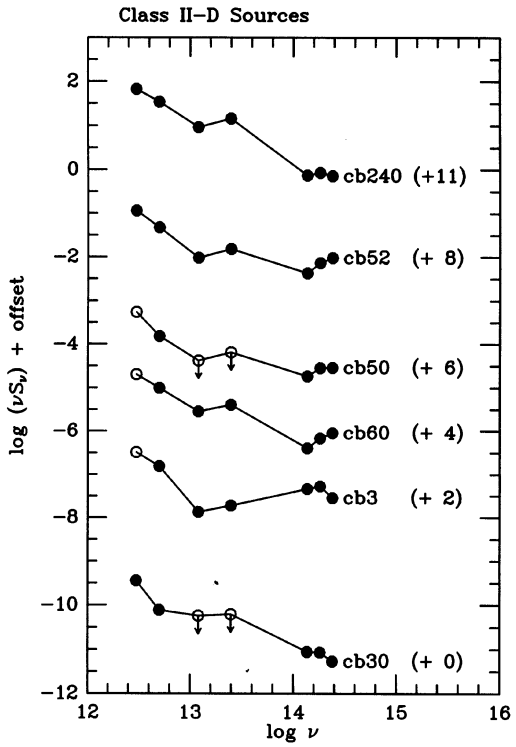

FIG. 7. Spectral energy distribution of the Class II YSOs.

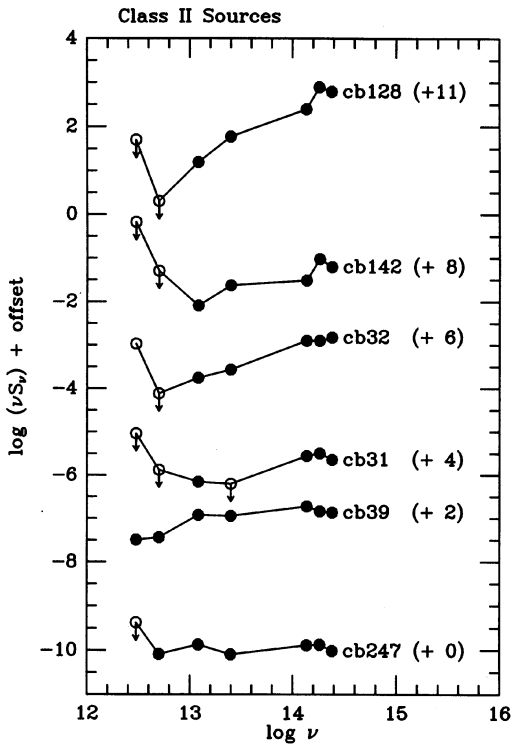

FIG. 8. Spectral energy distribution of Class II-D YSOs.

Figure 8 shows the SEDs for CB31YC1, CB32YC1, CB39YC1, and CB247YC1. Due to their flat SEDs or SEDs that rise towards shorter wavelengths, these sources are likely to be Class II sources. CB128YC1 and CB142YC1 have SEDs that rise rapidly towards shorter wavelengths. These sources could be extreme Class II sources close to becoming Class III sources.

In summary, of the 22 YSOs with infrared counterparts, 10 are Class I. Half of the remaining 12 sources are Class II and the other half are Class II-D. There are no examples of Class III sources in this sample.

4.2 Class I Sources

The most representative Class I YSOs (CB6YC1, CB34YC1, CB54YC1, CB205YC1, CB216YC1, CB230YC1, CB232YC1), have associated CO molecular outflows (Yun & Clemens 1992, 1994a) or near-infrared nebulosity (Yun & Clemens 1994b), and their SEDs are steeply decreasing functions of frequency. None of these objects have optical counterparts on the POSS (Yun & Clemens 1994b).

The SEDs of these sources are similar to the SEDs of other Class I sources found in the Taurus–Auriga molecular cloud (Myers *et al.* 1987; Kenyon *et al.* 1993). The youth of our objects is well established by the evidence (outflows, nebulosity) presented in previous papers (Yun & Clemens 1994b) and the steepness of their SEDs. Based on their SEDs, these sources are likely to be in the evolutionary stage identified by Adams *et al.* (1987) as deeply embedded protostars, surrounded by infalling dusty material, either in the form of an envelope or a disk and with a more or less collimated outflow (Adams & Shu 1986; Adams *et al.* 1987).

4.3 Class II and II-D Sources

Objects with a relatively flat SED ($\alpha \sim 0$ to 1) are often found to be classical T Tauri stars (e.g., Myers *et al.* 1987; Adams *et al.* 1987). In order to determine whether our Class II sources are similarly T Tauri stars, spectroscopic observations are required. In these objects, the infrared emission in excess of that from the stellar photosphere is thought to be produced in a circumstellar disk (Rucinski 1985; Strom *et al.* 1988). None of the Class II or Class II-D sources found here exhibit infrared nebulosity. Additionally, with exception of CB3YC1 and CB39YC1, none of the sources has an associated outflow.

5. SPECTRAL INDICES

Table 3 lists the spectral indices of the YSOs contained in Table 1. The 2/25 μm spectral indices are listed in column (2), the 12/25 μm spectral indices are listed in column (3), and the spectral indices obtained from an unweighted linear fit α (fit) to all the points in each spectrum are listed in

TABLE 3. Spectral indices and source classification.

YSO	Spectral indices			Source
	$\alpha_{2/25}$	$\alpha_{12/25}$	α (fit)	classification
(1)	(2)	(3)	(4)	(5)
CB3YC1	0.50	0.47	−0.33	II-D
CB6YC1	−0.88	−0.90	−0.85	I
CB30YC1	−0.78	0.11	−0.83	II-D
CB31YC1	0.08	0.66	−0.08	II
CB32YC1	0.81	0.59	0.38	II
CB34YC1	−0.46	−0.57	−0.71	I
CB39YC1	0.19	−0.06	0.34	II
CB50YC1	−0.34	0.60	−0.65	II-D
CB52YC1	−0.33	0.63	−0.55	II-D
CB54YC1	−1.32	−1.53	−1.60	I
CB60YC1	−0.81	0.49	−0.86	II-D
CB128YC1	1.14	1.82	1.01	II
CB142YC1	0.55	1.46	−0.17	II
CB188YC1	−0.47	−0.86	−0.71	I
CB205YC1	−1.04	−1.07	−1.18	I
CB214YC1	−1.01	−0.24	−1.35	I
CB216YC1	−0.82	−0.49	−0.77	I
CB230YC1	−0.26	−0.36	−0.89	I
CB232YC1	−1.37	−0.70	−1.14	I
CB240YC1	−1.03	0.63	−1.06	II-D
CB244YC1	−1.49	−0.55	−1.53	I
CB247YC1	−0.01	−0.70	−0.12	II

column (4). Column (5) indicates the spectral classification adopted here and described in the previous section.

Comparison of columns (2) and (4) reveals that, with the exception of CB142YC1, the two spectral indices, $\alpha_{2/25}$ and α (fit), show values that are very close to each other and thus contain the same information. Comparison of column (3) with columns (2) or (4), reveals that $\alpha_{12/25}$ gives similar information as $\alpha_{2/25}$ or α (fit) for Class I and Class II, but not for Class II-D sources. The latter type of sources tend to have negative values of $\alpha_{2/25}$ and α (fit) but positive values of $\alpha_{12/25}$. For sources in Classes I and II, conclusions about the spectral classification and the relative embeddedness of a source are similar, regardless of which type of spectral index, $\alpha_{2/25}$, $\alpha_{12/25}$, or α (fit), is used.

Comparison of columns (3) and (5) reveals that Class I sources, in particular, seem to be well identified by their 12/25 μm spectral indices, as illustrated in Fig. 9. This figure shows the cumulative fraction of sources with $\alpha_{12/25}$ smaller than or equal to a fixed value. The dashed line refers to Class I objects.

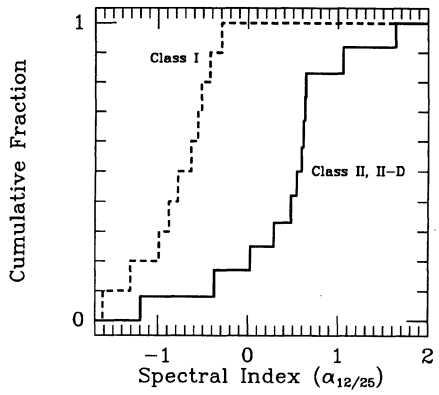

FIG. 9. Cumulative fraction of sources with $\alpha_{12/25}$ smaller than or equal to a fixed value. The dashed line refers to Class I objects. The solid line refers to Class II and II-D objects. All Class I objects have negative values of $\alpha_{12/25}$.

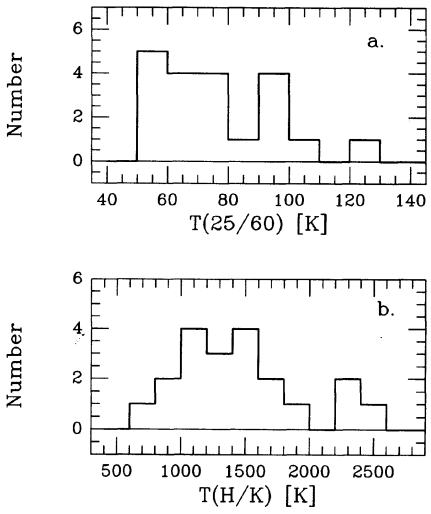

FIG. 10. Histograms of (a) the $T(25/60)$ and (b) $T(H/K)$, for the YSOs listed in Table 1 (except CB128YC1 and CB142YBC1). $T(25/60)$ shows a mean of 80 K and standard deviation of 30 K. $T(H/K)$ shows a mean of about 1400 K with a standard deviation of 500 K.

The solid line refers to Class II and II-D objects. All Class I objects have negative values of $\alpha_{12/25}$. Only one YSO with a negative value of $\alpha_{12/25}$ is not a Class I source. No such relation exists with $\alpha_{2/25}$ or α (fit).

6. CIRCUMSTELLAR DISKS, WARM DUST AND COLD DUST

Emission in the *IRAS* bands and emission in the near-infrared bands originate from dust with quite different temperatures. Such dust may be distributed among the very different physical structures associated with each protostar, namely the photosphere and the circumstellar envelope, or the dust emission may originate with spatially distinct zones contained in an active circumstellar disk. Although not strictly physical, these zones may be usefully characterized by the color temperatures of their *IRAS* and near-infrared emission.

Such color temperatures were calculated for the *IRAS* 25 and 60 μm bands and for the H and K near-infrared bands, assuming a dust emissivity law given by Draine & Lee (1984). The resulting distributions of the 25/60 color temperatures $T(25/60)$ and the H/K color temperatures $T(H/K)$ are shown in Fig. 10. The color temperatures of the cold dust range from about 50 to 120 K, with a mean of 80 K and standard deviation of 30 K. The color temperatures of the warm dust range from about 700 to about 2200 K. Most sources have $T(H/K)$ in the range of 1000 to 1600 K. The mean of the distribution is about 1400 K with a standard deviation of 500 K. These values are similar to those obtained by Persi *et al.* (1990) in their survey of YSOs in southern dark clouds. Two sources, CB128YC1 and CB142YC1, were excluded since they have $T(H/K)$ of 3000

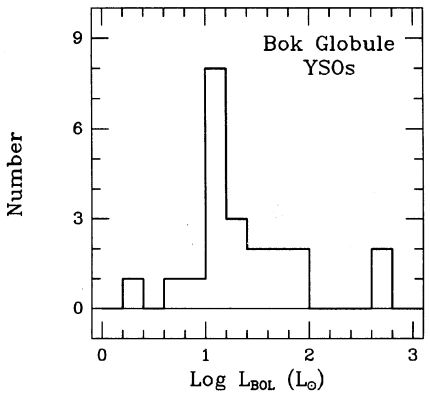

FIG. 11. Distribution of luminosities of the YSOs assuming a mean distance to the sources of 600 pc (except for CB3YC1 and CB205YC1 whose distances have been previously estimated).

K or higher. These two sources, being extreme Class II sources, may not have circumstellar dust and the high color temperatures are more likely due to the stellar photosphere than to disk emission.

Theoretical models of flat spectrum ($\alpha \sim 0$) sources have employed spatially thin, optically thick circumstellar disks (Adams *et al.* 1988) with disk radial temperature gradients of the form $T(r) \propto r_D^{-q}$, where r_D is the disk radius and q is in the range of 0.5 to 0.75. If we assume that an optically thick disk around each of our YSOs is responsible for producing the observed emission (a weak assumption for the colder sources), with a radial temperature distribution in the form of a power law, $T \propto r^{-q}$, the $\alpha_{2/25}$ spectral indices listed in Table 3 correspond to exponents q in the range of 0.36 to 0.70, via the expression $\alpha = 4 - 2/q$ (see Adams *et al.* 1988).

7. LUMINOSITIES

An estimate of the bolometric luminosities of the YSOs can be obtained assuming a mean distance of 600 pc to all sources (Clemens & Barvainis 1988), with exception of CB3YC1 ($d \sim 2.1$ kpc; Yun & Clemens 1994a) and CB205YC1 ($d \sim 2.5$ kpc; Xie & Goldsmith 1990). The luminosity distribution is shown in Fig. 11. The luminosities were determined by integrating over the values of the J, H, K, 12, 25, 60, and 100 μm fluxes, excluding, however, the *IRAS* upper limits. Given the large uncertainty in the individual distances, we did not correct for the contribution to the luminosity beyond the *IRAS* longest wavelength. If we assume that the SEDs peak at wavelengths ≤ 100 μm, these corrections have been found to be small (<30%, Myers *et al.* 1987; Kenyon *et al.* 1990).

The two sources in Fig. 1 with the highest luminosities are CB3YC1 and CB205YC1, whose distances are much larger than the adopted mean of 600 pc. These sources are likely to be the most luminous in the sample. Of all the sources in the CB sample, these sources were two of the four brightest 100 μm sources and are likely intermediate mass YSOs. The source in Fig. 11 with the lowest luminosity is CB214YC1.

The log-based mean luminosity for the sample is 23 $L_\odot$ with a standard deviation of 13 $L_\odot$. These values are about one order of magnitude higher than corresponding values for embedded sources in Taurus (Myers *et al.* 1987). Given the large uncertainty in the distances to the sources, the values of these luminosities should be regarded with caution.

An estimate of the typical masses of the objects was obtained following a procedure similar to the one used by Yun & Clemens (1990). YSOs typically exhibit enhanced luminosities relative to main-sequence stars of the same mass (Adams & Shu 1985; Stahler 1988). Therefore, in order to obtain the luminosities of a main-sequence star of the same mass, the luminosities of a YSO need to be scaled down by a factor of 5–10, depending on the youth of the objects. Given that a large fraction of the YSOs in our sample are Class I or Class II-D, a decrement factor of 10 was used here. The mass of a typical object (with luminosity equal to the mean of 23 $L_\odot$) was found to be ~ 1 $\mathcal{M}_\odot$. An estimate of the sensitivity limit (3σ detection across all seven bands: *JHK* and *IRAS*) yields a bolometric luminosity of 2.8 $L_\odot$. Both this value and the lower luminosity limit of Fig. 11 correspond to a mass of ~ 0.7 $M_\odot$. As in Yun & Clemens (1990), we conclude that we may not have found all the embedded low-mass stars in the globules, or that very low mass stars are uncommon.

8. SUMMARY

Photometry of the near-infrared images obtained towards the YSOs provided near-infrared magnitudes and fluxes of these objects.

The results of the photometry (near-infrared colors) together with the coordinates of the objects were used to identify the most likely near-infrared counterparts to the YSOs.

Broadband spectral energy distributions for the YSOs were established and plotted. The sources were classified according to the shapes of their SEDs.

The SEDs confirmed the YSO nature of the 22 *IRAS* PSC sources exhibiting identifiable near-infrared counterparts. Of these 22, 10 are Class I. Half of the remaining 12 sources are Class II and the other half are Class II-D.

For Class I and Class II sources, both the 12/25 μm spectral index and the 2/25 μm spectral indices give the same information about the embeddedness and type of YSO.

Class I sources seem to be particularly well identified by the 12/25 μm spectral index.

REFERENCES

Adams, F. C., & Shu, F. H. 1985, ApJ, 296, 655
Adams, F. C., & Shu, F. H. 1986, ApJ, 308, 836
Adams, F. C., Lada, C. J., & Shu, F. H. 1987, ApJ, 312, 788
Adams, F. C., Lada, C. J., & Shu, F. H. 1988, ApJ, 326, 865
Draine, B. T., & Lee, H. M. 1984, ApJ, 285, 89
Elias, J. H., Frogel, J. A., Matthews, K., & Neugebauer, G. 1982, AJ, 87, 7
Ellis, T., *et al.* 1992, Proceedings of the Society of Photo-Optical Instrumentation Engineers
Emerson, J. P. 1988, Formation and Evolution of Low-Mass Stars, edited by A. K. Dupree and M. T. V. T. Lago (Reidel, Dordrecht), p. 21
Johnson, H. L., MacArthur, J. W., & Mitchell, R. E. 1968, ApJ, 152, 465
Kenyon, S. J., Whitney, B. A., Gomez, M., & Hartmann, L. 1993, ApJ, 414, 773
Koornneef, J. 1983, A&A, 128, 84
Lada, C. J. 1988, Proc. NATO/ASI, Galactic and Extragalactic Star Formation, edited by R. E. Pudritz and M. Fich (Reidel, Dordrecht), p. 5
Lada, C. J., & Wilking, B. A. 1984, ApJ, 287, 610
Lada, C. J. 1991, The Physics of Star Formation and Young Stellar Evolution, edited by C. Lada and N. Kylafis (Reidel, Dordrecht), p. 329
Lada, C. J., & Adams, F. C. 1992, ApJ, 393, 278
Myers, P. C., Fuller, G. A., Mathieu, R. D., Beichman, C. A., Benson, P. J., Schild, R. E., & Emerson, J. P. 1987, ApJ, 319, 340
Persi, P., Ferrari-Toniolo, M., Busso, M., Origlia, L., Robberto, M., Scaltriti, F., & Silvestro, G. 1990, AJ, 99, 303
Rieke, M. J., Montgomery, E. F., Rieke, G. H., Vural, K., Blessinger, M., & Kleinhans, W. 1989, Proceedings of the Third Infrared Detector Technology Workshop, edited by C. R. McCreight, p. 321
Rucinski, S. M. 1985, AJ, 90, 2321
Rydgren, A. E., & Zak, D. 1987, PASP, 99, 41
Stahler, S. W. 1988, ApJ, 332, 804
Thompson, R., Rieke, M., Young, E., McCarthy, D., Rasche, R., Blessinger, M., Vural, K., & Kleinhans, W. 1989, Proceedings of the Third Infrared Detector Technology Workshop, edited by C. R. McCreight, p. 331
Wilking, B. A., Lada, C. J., & Young, E. T. 1989, ApJ, 340, 823
Xie, T., & Goldsmith, P. F. 1990, ApJ, 359, 378
Yun, J. L., & Clemens, D. P. 1990, ApJ, 365, L73
Yun, J. L., & Clemens, D. P. 1992, ApJ, 385, L21
Yun, J. L., & Clemens, D. P. 1994a, ApJS, 92, 145
Yun, J. L., & Clemens, D. P. 1994b, AJ, 108, 612